

A Microring as a Reservoir Computing Node: Memory/Nonlinear Tasks and Effect of Input Non-ideality

Davide Bazzanella,* Stefano Biasi, Mattia Mancinelli, and Lorenzo Pavesi

Nanoscience laboratory, Department of Physics, University of Trento, Via Sommarive 14, 38123, Trento, Italy

(Dated: March 15, 2022)

The nonlinear response of an optical microresonator is used in a time multiplexed reservoir computing neural network. Within a virtual node approach combined with an offline training through ridge regression, we solved linear and nonlinear logic operations. We analyzed the nonlinearity of the microresonator as a memory between bits and/or as a neural activation function. This is made possible by controlling both the distance between bits subject to the logical operation and the number of bits supplied to the ridge regression. We show that the optical microresonator exhibits up to two bits of memory in linear tasks and that it allows solving nonlinear tasks providing both memory and nonlinearity. Finally, we demonstrate that the virtual node approach always requires a comparison of the reservoir's performance with the results obtained by applying the same training process on the input signal.

Keywords: Optical neural systems, Neural networks, Nonlinear optics, Integrated optics, Silicon microresonators

I. INTRODUCTION

Nowadays, artificial neural network (ANNs) are able to carry out tasks of remarkable complexity and abstraction. These statistical models are usually created by analysing extensive datasets or by repeating a training procedure a substantial number of times. Thanks to the recent exponential increase in computational power of general purpose accelerators, derived from graphic processing unit (GPU) architectures, it has been possible to create and emulate ANNs of increasing size, in a shorter time and more efficiently [1, 2]. However, a fundamental difference between ANNs and common computers still remains: in the former, computation occurs in parallel at each node, while in the latter information is elaborated in CPUs and GPUs only. Due to this discrepancy, computers are not the most energy efficient means for creating and running ANNs.

In order to overcome these limitations, hardware implementations of ANNs with different combinations of architectures and physical substrates have been attempted [3–11]. Reservoir computing (RC) with photonics is an interesting approach to the matter, as it combines the bandwidth, parallelism, and low energy consumption proper of photonics and the weak requirements of RC based ANNs [12]. In these ANN, a recurrent untrained network of randomly interconnected nonlinear neurons (*the reservoir*) is interfaced through trainable connections with a single layer of output neurons (*the output perceptron*). In photonics, the *reservoir* that increases the dimensionality of the RC input data can be implemented either by a big number of simpler nodes [13] or by a single much more complex and highly nonlinear element [14]. This is especially important for integrated photonics, whose fundamental blocks have limited cas-

cadability.

An approach to photonic RCs aims at using a single photonic device to create the *reservoir*, whose single output is sampled at different times, creating a set of virtual nodes. This method is called time multiplexing, and require memory storage of the virtual nodes. Often, the output layer is carried out offline, after the optical readout has been converted to digital signals [5, 14, 15]. The final network output is computed as a weighted sum of the status of the virtual nodes. Therefore, this RC implementation can be easily trained by using a simple ridge regression. This procedure allows the study of promising optical reservoir, without the additional burden of integrating the output regression layer.

Within this approach particular care should be placed on the network testing phase when binary inputs are used. In fact, the optical binary input signal differs from the ideal binary input because of the non-ideal response of the optical bit generation stage, usually composed by a continuous wave (CW) laser and one or more electro-optic (E/O) modulators. For this reason, as we will show in this article, it is fundamental to compare the performance of the RC system to that of the isolated readout layer applied directly to the optical input.

In this work, we studied the implementation of a silicon microresonator as a reservoir. Referring to our recent work [16], a binary time sequence of bits is injected into the system at different bitrates, average powers, and detuning with respect to the resonant frequency. As a result, the nonlinearity of the microresonator, which follows the free carrier and temperature dynamics [17], encode the information in the output response. The free carrier recombination and the temperature cooling provide the intrinsic fading memory to the network. Note that here, at difference with [16], we use a single pulsed input optical signal. Training the system by means of an off-line ridge regression, allows treating different binary tasks, isolating the role of the nonlinearity of the microresonator on the fading memory between bits and on the nonlinearity

* davide.bazzanella@unitn.it

(activation function) imprinted on the output response.

The paper is organized as follows. To begin with, we present in Section II the basic principle of the network, explaining the implementation of a microresonator/bus waveguide system as a reservoir. We describe the encoding of information into the input signal and the training process. We then present the experimental realization in Section III, where we discuss the samples and the experimental setup, showing how the data were acquired. In Section IV we show the experimental results obtained in the test process, discussing the role of the nonlinearity induced by the microresonator. Finally, we summarise our main results in Section V.

II. THEORY AND BASIC PRINCIPLE

A single microresonator in the add-drop configuration is used as a reservoir, implementing virtual nodes through the time multiplexing technique [18]. The number of virtual nodes N_v is determined by the bit duration T_b and the virtual node temporal separation (δt), i.e. $N_v = T_b/\delta t$. Note that in this case, T_b is determined by the used bit rate and is not connected to any delay-loop as in the classical architectures [19, 20].

The input signal is an optical binary sequence \mathbf{I}_N of length N , encoding the logical binaries 0 and 1 with the lowest and maximum optical intensities of a single frequency pump laser, respectively. The input optical signal is then a sequence of bits \mathbf{b}_j^i , each of which is composed by a N_v number of samples i_j , or virtual nodes:

$$\mathbf{I}_N = (\mathbf{b}_1^i, \dots, \mathbf{b}_j^i, \dots, \mathbf{b}_N^i) \quad (1)$$

$$\mathbf{b}_j^i = (i_1, \dots, i_j, \dots, i_{N_v}). \quad (2)$$

The possibility of varying both the frequency and power of the pump laser allows to study the effects of the microring resonator nonlinear response [17]. This nonlinearity, applied to the input signal, is due to either or both the dynamics of the free carrier population density and the temperature within the ring's waveguides. The pump laser generates free carriers through Two Photon Absorption (TPA) which, in turn via free carrier dispersion, generates a blue shift of all the resonant frequencies of the microresonator. On the other hand, the temperature of the microresonator increases due to free carrier relaxation and light absorption in the waveguide material. This induces a red shift of all the resonant frequencies due to the thermo-optic effect. The two effects are characterized by different relaxation times and power dependences. Then, depending on the frequency detuning (difference between the pump laser frequency and the microring resonant frequency), the input power and the bit rate, one of these phenomena can overcome the other or both can occur leading to an unstable scenario characterized by a self-pulsing regime [21, 22]. As a result, such nonlinearities define the connection between the virtual nodes [16], providing both the memory capability and the nonlinearity to the reservoir.

AND	0	1	OR	0	1	XOR	0	1
	0	0	0	0	1	0	0	1
	1	0	1	1	1	1	1	0

TABLE I: Truth table for AND, OR, and XOR operations.

The output bit \mathbf{b}_j^o is measured at the output port of the system, i.e. the microresonator transmitted light is detected and sampled each δt yielding the virtual nodes status o_j . These output bits are arranged in the hidden nodes matrix:

$$\mathbf{X} = (\mathbf{b}_1^{oT}, \dots, \mathbf{b}_j^{oT}, \dots, \mathbf{b}_N^{oT}) \quad (3)$$

$$\mathbf{b}_j^o = (o_1, \dots, o_j, \dots, o_{N_v}), \quad (4)$$

where each column \mathbf{b}_j^o contains N_v virtual nodes. Then, offline, the RC output \mathbf{Y} is obtained by a simple matrix multiplication of the hidden nodes matrix with a weight matrix \mathbf{W} , i.e. $\mathbf{Y} = \mathbf{X}\mathbf{W}$

The reservoir training is obtained by determining the weight matrix $\tilde{\mathbf{W}}$, which allows predicting the target \mathbf{Y}_T . This problem is solved by regularized least squares (ridge regression), exploiting the `firtrlinear` algorithm of Matlab. Here, the regularization parameter λ is defined by a 5-fold cross validation, so that the result of the ridge regression is the matrix $\tilde{\mathbf{W}}$ which minimizes the regularized least square error.

The binary tasks studied are the logical operations AND, OR, and XOR, whose truth tables are reported in Table I and which are carried out on the present bit with a bit in the past. To explicit the bits on which the operation is carried out, we use the following notation: "LO n_1 with n_2 R-bit", where LO is the logical operation, n_1 is the distance between the bits on which the LO is performed (the present and the past bits), and n_2 is the number of bits, starting from the present one, provided to the ridge regression (the R-bits). For example, "AND 2 with 2 R-bits" means to perform an AND logical operation between the \mathbf{b}_j^i and \mathbf{b}_{j-2}^i , providing the virtual nodes of \mathbf{b}_j^o and \mathbf{b}_{j-1}^o to the ridge regression algorithm. For each task the following cases were investigated:

- logical operation between bits \mathbf{b}_j^i and \mathbf{b}_{j-1}^i , providing to the ridge regression the bit \mathbf{b}_j^o or $\mathbf{b}_{j-1}^o \& \mathbf{b}_j^o$, see Fig. 1a;
- logical operation between bits \mathbf{b}_j^i and \mathbf{b}_{j-2}^i , providing to the ridge regression the bit \mathbf{b}_j^o or $\mathbf{b}_{j-1}^o \& \mathbf{b}_j^o$ or $\mathbf{b}_{j-2}^o \& \mathbf{b}_{j-1}^o \& \mathbf{b}_j^o$, as shown in Fig. 1b;
- logical operation between bits \mathbf{b}_j^i and \mathbf{b}_{j-3}^i , providing to the ridge regression the bit \mathbf{b}_j^o or $\mathbf{b}_{j-1}^o \& \mathbf{b}_j^o$ or $\mathbf{b}_{j-2}^o \& \mathbf{b}_{j-1}^o \& \mathbf{b}_j^o$ or $\mathbf{b}_{j-3}^o \& \mathbf{b}_{j-2}^o \& \mathbf{b}_{j-1}^o \& \mathbf{b}_j^o$, see Fig. 1c.

Varying the distance between the bits subject to the logical operation allows testing the memory imprinted on the output signal by the microresonator. We can supply to the ridge regression the current bit only, so that the

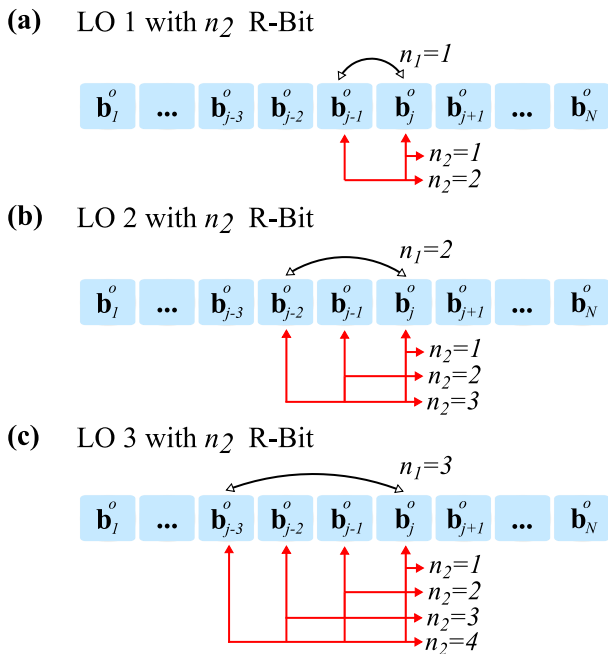


FIG. 1: Sketch representing the three cases on which we tested the logical operations. n_1 indicates the distance between the bits on which the logical operation (LO) is performed and n_2 is the number of bits provided to the ridge regression in the training procedure. Note that the flow of bits is such that the past bits ($b_{j-n_1}^o$) are processed by the microresonator before the present bit (b_j^o), i.e. the bit flow is inverted with respect to the time flow which is indicated in the figure.

system has to provide the memory to the regression, or we can make all the bits in the operation directly available to the regression. In the last scenario, the attention can be focused on the nonlinearity of the microresonator imprinted on the output signal.

Despite the apparent simplicity of the logical operation AND, OR and XOR, these tasks unveil the main characteristics of the reservoir: the nonlinear transformation of the input and the presence of fading memory [16, 23–25]. AND and OR, are linear tasks, and therefore, do not require a nonlinear response for their solution. However, in order to solve these linear tasks it is necessary for the system to provide memory between the bits. This allows isolating the role of optical nonlinearity on the memory between the distinct bits. Differently, the solution of the logical XOR requires both: nonlinearity of the response and memory between the different bits considered in the task. As a result, we can distinguish between the two contributions by providing or not providing memory to the ridge regression during the training process.

III. SAMPLES AND EXPERIMENTAL REALIZATION

The device under test (DUT) was a microring resonator with a radius of $7\ \mu\text{m}$ in the add-drop configuration, which has been fabricated at the CEA-Leti facility on a SOI (silicon-on-insulator) wafer. The top-view of the sample is shown in the sketch of Fig. 2a. Briefly, the DUT is composed by single mode channel silicon waveguides with a width and height of $450\ \text{nm}$ and $220\ \text{nm}$, respectively. Two bus waveguides are point-coupled to the microring with a gap of $200\ \text{nm}$. The normalized transmittance spectrum of a resonance measured at the drop port is shown in Fig. 2b. From this response it is possible to estimate a quality factor of about 6×10^3 at a frequency of $193.5\ \text{THz}$. As a result, the photon lifetime in the cavity is equal to $4.93\ \text{ps}$ [26]. Differently, the free carrier lifetime τ_{FC} is about a few nanosecond, as reported in literature for similar structures [27–30], while the thermal relaxation time is about $100\ \text{ns}$ [31, 32]. It is worth noting that this τ_{FC} is about one order of magnitude shorter than the value estimated in our works [16, 17], where $\tau_{FC} = 45\ \text{ns}$ on IMEC fabricated microresonators. This means that the transient phenomena occur at a temporal scale 10 times shorter in our DUT with respect to what was found in [16]. Indicatively, at $8\ \text{dBm}$ the response of these DUTs can be considered linear at all frequencies. Increasing the average input optical power, the nonlinear effects become more significant. At the highest values of input power, earlier for small detuning values and later for larger detunings, self-pulsing happens. For example, an input signal in resonance with the ring with an average power of $16\ \text{dBm}$ triggers the self-pulsing effect. The possibility of varying the frequency of the pump laser from negative to positive detunings, allows forcing a particular nonlinear effect. In fact, negative detuning induces free carriers through TPA, while positive detuning favors the thermo-optic effect. However, with a fixed input frequency at high input power, the microresonator exhibits a nonlinearity that is effectively an interplay between the two effects [16].

The experimental setup is sketched in Fig. 2c. The pump is a CW tunable laser, which operates in a range spanning from $191.5\ \text{THz}$ to $196.25\ \text{THz}$ (CWTL). Its intensity is modulated by an electro-optic IQ modulator (EOM), controlled by a $65\ \text{GSa/s}$ Arbitrary Waveform Generator (AWG), in order to create the desired binary sequence. This signal passes through a fiber-optic splitter which allows detecting the input pump by a fast photodiode detector (PD1). The remaining of the pump is adjusted in polarization by a polarization control (PC), is amplified by an Erbium Doped Optical Amplifier (EDFA1), and attenuated again to obtain the required power by an electronic Variable Optical Attenuator (VOA1). The resulting signal is fed to the sample through the coupling between a single mode fiber and the input grating coupler. Similarly, another single mode fiber is coupled to the output grating coupler to read the

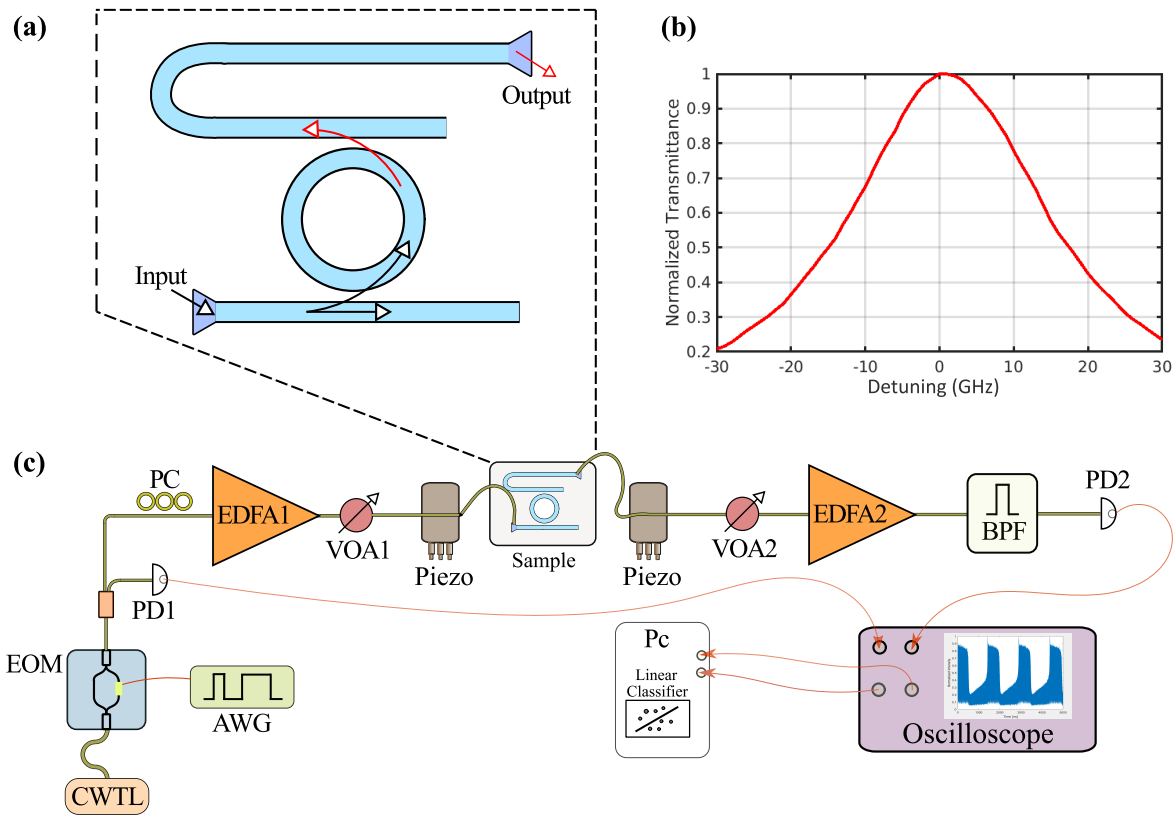


FIG. 2: (a) Sketch of the microring resonator in the add-drop configuration. (b) Normalized transmission spectrum around the resonance frequency. The detuning is the frequency difference between the laser frequency and the microring resonant frequency of 193.5 THz. (c) Diagram of the experimental setup. CWTL: Continuous Wave Tunable Laser, AWG: Arbitrary Waveform Generator, EOM: Electro-Optic Modulator, PD: Photodetector, PC: polarization control, VOA: Variable Optical Attenuator, EDFA: Erbium Doped Optical Amplifier, BPF: Band Pass Filter, Pc: Personal computer.

output signal. A correct alignment is ensured by a three axis linear piezoelectric stage on both the input and output. The signal collected at the output is injected into a second electronic Variable Optical Attenuator (VOA2), re-amplified by a second Erbium Doped Optical Amplifier (EDFA2), and cleaned from the optical noise with a tunable band-pass filter (BPF). The resulting output is detected by a second photodiode (PD2). At the end, a 4-channel 40 GSa/s oscilloscope monitors and records the input and output optical waveform. A Personal computer (Pc) elaborates the traces, and performs an offline training and test of the network by using Matlab.

The input signal injected into the microresonator consists of a Pseudo Random Binary Sequence (PRBS) of order 8 and length 255, repeating indefinitely. Its characteristics can be changed by varying three distinct variables: bitrate, detuning (input minus resonant frequency) and average power. Precisely, the variables span over the following values:

- bitrate: 20, 40, 50, 80, 100, 200, 250, 400, 500, 800, 1000, 2000, and 4000 Mbps;
- detuning: $-30, -25, -20, -15, -10, -5, 0, 5, 10, 15, 20, 25,$ and 30 GHz;

- input Power: 8, 9, 10, 11, 12, 13, 14, 15, 16, 17, and 18 dBm.

For each combination of bitrate, incident power, and frequency detuning, the input and the output optical signals are acquired. The second amplification stage, consisting of the EDFA2 and of the VOA2, keeps constant the average power at PD2, avoiding marked changes in the signal-to-noise ratio (SNR), which could otherwise compromise the performance comparison between different combination of parameters.

In the time multiplexing approach, knowledge of the input is crucial to verify that the experimental apparatus alone is not able to solve the task. Indeed, both the signal generation and detection stages can distort the ideal PRBS by imprinting spurious nonlinearities and adding unwanted memory due to their finite electronic bandwidth. Therefore, the oscilloscope records both the input (the PD1 signal) and the output (the PD2 signal) optical waveforms, with a fixed sampling rate of 20 GSa/s. As a result, the sampling rate of the oscilloscope defines the number of samples in each bit for each bitrate. Specifically, it spans from a maximum of 1000 to a minimum of 5, for 20 Mbps and 4000 Mbps, respectively.

The acquired samples per bit are re-binned to obtain N_v^d virtual nodes: they are divided into the desired number of bins and for each one is performed the average. For example, assuming a $N_v^d = 10$, each bit would have 10 virtual nodes obtained as follows:

1. 10 samples obtained by re-binning the experimental data, at input bitrates from 20 Mbps to 1000 Mbps;
2. all the 10 samples acquired, at 2000 Mbps;
3. the values of the five samples acquired and zero for the remaining 5 nodes, at 4000 Mbps.

The minimization of the regularized square error, i.e. the solution of the system $\mathbf{Y}_T = \mathbf{X}\tilde{\mathbf{W}}$, is performed on both the input and the output signals by processing them as a function of the maximum desired number of virtual nodes (N_v^d).

IV. EXPERIMENTAL RESULTS

For each combination of the three input variables (see Section III), we performed the training for different logical operations on both the input and the output optical signals, i.e. we detected the optical data and then we applied the ridge regression on the digital data. When the training is performed on the output optical signal we are using the whole microring based RC network. We studied a number of virtual nodes equal to 3, 4, 5, 10, 15, 20, and 30. The tasks have been implemented following the cases reported in Section II. Then, the performance of the network has been assessed by estimating the bit error rate (BER).

Among the several results, we selected a few instructive cases, which reveal the effect of the nonlinearity of the microring resonator. We report the results separating them according to the logical operation. In each case, we show three contour maps as a function of the input bitrate and the frequency detuning. The first map shows the best value of the BER ($\text{BER}_{\text{out}}^b$) obtained by the RC network with the input power which ensures the best performance. The second map shows the lowest value of input power at which $\text{BER}_{\text{out}}^b$ is achieved. The third one shows the ratio RB between the BER^b estimated when the ridge regression is applied on the input optical data (BER_{in}^b) or on the output optical data ($\text{BER}_{\text{out}}^b$): $RB = \text{BER}_{\text{in}}^b / \text{BER}_{\text{out}}^b$. The color code for the ratio RB is given on the map with two different color-ranges: one from blue to yellow, the other from black to white. The first highlights where the microring introduces an improvement of the performance. Specifically, the yellow indicates a better result of the RC network, and therefore, defines the regions of performance improvement given by the microring nonlinearity. The other color range is a gray scale that shows where the results of the RC are worse than barely performing the ridge regression on the input optical data. In particular, the black color indicates that RB is equal to one, i.e. the task is solved with

the same BER either when the input optical data are processed or when the output optical data are processed, while the gray and white colors indicate regions in which $\text{BER}_{\text{out}}^b$ is worse than BER_{in}^b . This means that the nonlinear response of the microring does not introduce any advantage but it is only detrimental. For the sake of clarity, all the maps are represented with a logarithmic (\log_{10}) scale.

Moreover, in the map of the $\text{BER}_{\text{out}}^b$ we define with red dots the points where the results reach the statistical limit. The same points are replicated in the third map, using empty red dots and crosses when the statistical limit is reached by processing the input and output optical signals, respectively.

A. Linear logical operations: AND and OR

Logical AND and OR tasks are linearly separable (see Table I for the truth tables), hence the nonlinearity of the microresonator provides only the memory of the past bit for the operation. As a result, varying the distance between the bits subject to the logical operation allows testing the memory capability of the network.

1. AND 1 with 2 R-bits and $N_v^d = 5$

The “AND 1 with 2 R-bits” is a linear task where we provide both bits - the current bit and the past one - to the ridge regression. In this case, we expect to be able to solve the task both by the RC and by processing only the input optical signal. The results confirm these expectations and are shown in Fig. 3.

The system is in fact able to solve the task without errors in almost all configurations, as we can see from the top panel. However, we can observe a slight deterioration of the the BER in some isolated regions, probably due to lower SNR (signal to noise ratio). The absolute minimum BER^b value is equal to $10^{-3.4}$ and the statistical limit is achieved at all input bitrates apart from 2000 Mbps. Looking at the power map (see middle panel), there is no clear dependence of the BER^b on the frequency detuning. Furthermore, the best BER results are found at low values, whereas, the lowest performance is characterized by high powers. As expected, the bottom map shows that the performance of the RC is equal to that achieved by processing only the input optical signal almost everywhere. For bitrates around 2000 and 4000 Mbps $\text{BER}_{\text{out}}^b$ is even worse than BER_{in}^b . In these cases, the microresonator distort the information carried by the input and it is, therefore, detrimental to the task resolution.

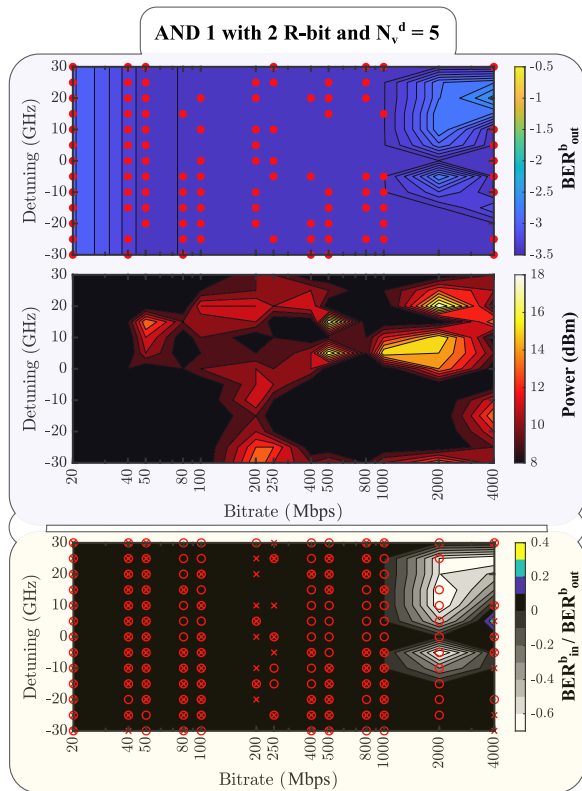


FIG. 3: Maps as a function of the frequency detuning and input bitrate for AND 1 with 2 R-bit and $N_v^d = 5$. **(top)** BER estimation from the RC network at the power which ensures the best network performances; **(middle)** the power at which the $\text{BER}_{\text{out}}^b$ values in the first panel are achieved; **(bottom)** the ratio between BER_{in}^b and $\text{BER}_{\text{out}}^b$. All the values are given in a logarithmic scale.

2. AND 1 with 1 R-bit and $N_v^d = 5$

Similarly to the previous example, “AND 1 with 1 R-bit” is a linear task. However, differently than before, we provide now only the current bit to the ridge regression. The nonlinearity of the microring resonator, then, must provide memory of the past bit to the regression. Indeed, the past bit has been injected into the microring resonator, as shift in temperature or free carrier population, to influence the current bit transmission. The results are shown in Fig. 4.

The best BER estimated (top panel) shows low values for a vast portion of the bitrate-detuning parameter space, with an absolute minimum of $10^{-3.4}$. Moreover, the statistical limit (red dots) is reached at several frequency detuning values for bitrates ranging from 20 Mbps to about 500 Mbps. From this map alone we cannot infer a clear dependence of the $\text{BER}_{\text{out}}^b$ as a function of the frequency detuning. On the contrary, the power at which $\text{BER}_{\text{out}}^b$ is obtained (see middle panel) shows that at zero detuning the system solves the task even at low power, while away from the resonance it re-

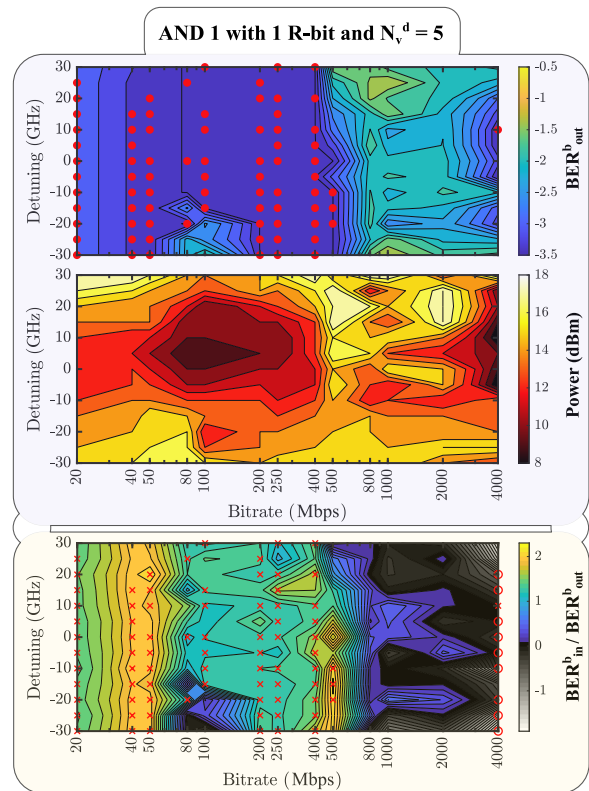


FIG. 4: Same maps of Fig. 3 for AND 1 with 1 R-bit and $N_v^d = 5$.

quires higher incident powers. Lastly, from the bottom panel, showing the ratio RB , we can observe wide regions of marked improvement in the performance of the RC network with respect to processing only the input optical signal. This improvement extends roughly from 20 Mbps to 500 Mbps and reaches about two orders of magnitude in the yellow region between 40 and 50 Mbps. On the other hand, for higher bitrates (approximately from 1000 Mbps to 4000 Mbps) the results provided by the RC network equals those obtained by processing only the input optical signal (dark gray and black regions). The extreme case occurs at 4000 Mbps, where the ridge regression achieves the statistical error limit on processing the input optical signal, only. This confirms what we have seen in the previous case, where at high input bitrates the nonlinearity distort the signal, and therefore, it does not play a memory role. Furthermore, this verifies the presence of unwanted memory in the signal, due to either the generation or the detection stages, even capable, in this extreme case, of solving the task.

3. AND 2/3 with 1 R-bit and $N_v^d = 5$

By increasing the distance between the bits on which the logical AND operation is performed, more memory capacity of the reservoir is required. Figure 5 shows the

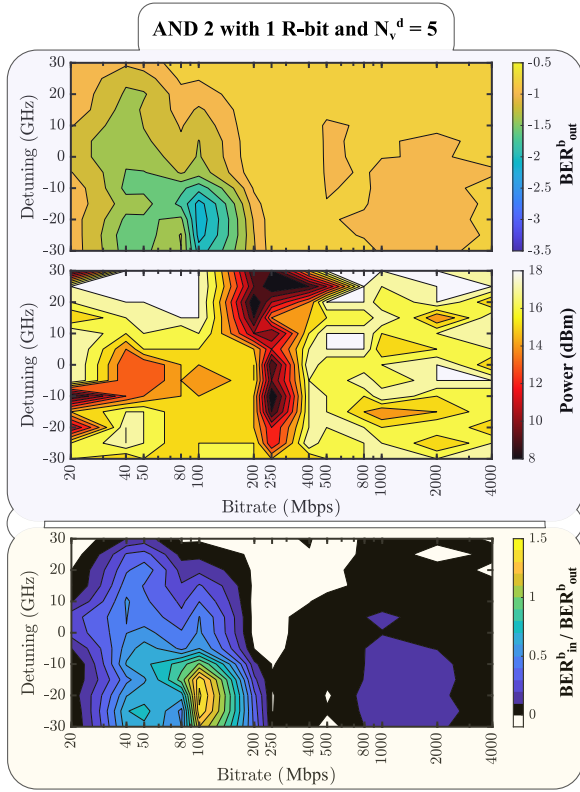


FIG. 5: Same maps of Fig. 3 for AND 2 with 1 R-bit and $N_v^d = 5$.

results for AND 2 with 1 R-bit and $N_v^d = 5$.

In this case, the map of the BER_{out}^b (top panel) exhibits a marked region where the RC network solves the task. In particular, there is a minimum BER of about 10^{-2} at a bitrate of 100 Mbps and a frequency detuning equal to -20 GHz. The map in the middle panel of Fig. 5 shows that this value is obtained at powers which ensure a nonlinear response of the microring resonator. It is worth noting that the RB ratio map (bottom panel) also highlights this area of better performance. Specifically, the maximum performance improvement shows a ratio of about $10^{1.5}$ at a bitrate of 100 Mbps. It seems that the best value of the RB occurs in the presence of a nonlinear effect related to free carrier dynamics. In fact the best performance of the output is obtained around 100 Mbps at negative detuning with approximately 15 dBm.

Moreover, there is a small region where the RC network performs slightly better than the bare processing of the input optical signal for bitrates of 1000 and 2000 Mbps, but the improvement is extremely small ($10^{0.1}$). It is important to notice that the area of lower RB coincides to an area of low input power. This suggests that in these cases the system nonlinearities are detrimental.

From these results, we find that the microring resonators used as a reservoir exhibits a memory of two bits. Interestingly, increasing the number of virtual nodes, the regions where the BER_{out}^b is lowest remain unchanged

while the minimum BER^b value progressively decreases until it reaches a value of about $10^{3.4}$ for 30 virtual nodes. In this case, RB gets to a maximum value of $10^{-2.6}$.

In the AND 3 with 1 R-bit and $N_v^d = 5$ task, the absolute value of BER_{out}^b reaches a minimum value of approximately 10^{-1} at a bitrate of 100 Mbps and -20 GHz detuning where RB equals to $10^{0.26}$. It is clear that the nonlinear response of the microresonator is not sufficient to guarantee the memory capacity needed to solve the 3-bit delay task.

B. Nonlinear logical operation: XOR

The XOR logical operation is not linearly separable and, therefore, it cannot be successfully solved using only the ridge regression. Furthermore, the solution of the n -bit delay XOR requires also a memory capability corresponding to a n -bit delay between the input bits.

1. XOR 1 with 1 R-bit and $N_v^d = 5$

The XOR 1 operation requires both nonlinearity and memory, however, because it is carried out on two contiguous bits, the memory may come from the intersymbolic interference already present in the input optical

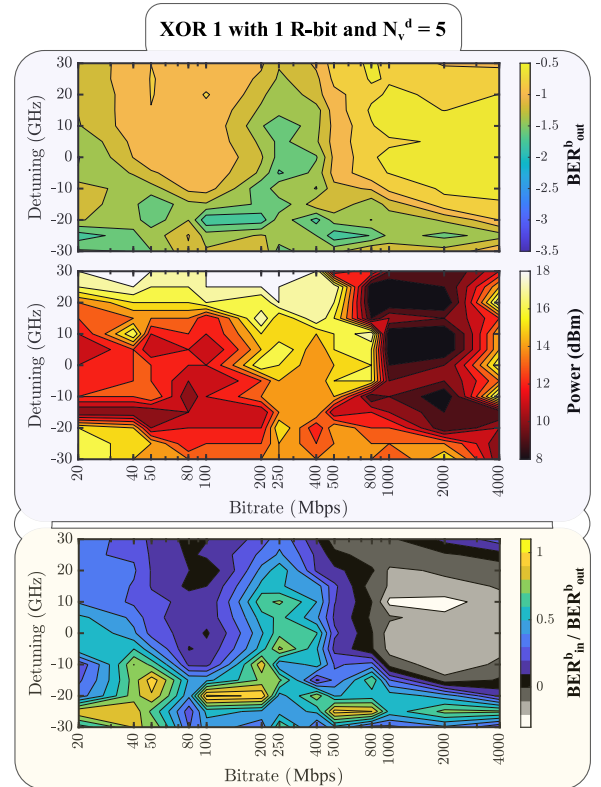


FIG. 6: Same maps of Fig. 3 for XOR 1 with 1 R-bit and $N_v^d = 5$.

signal. The values of RB should clarify the role of the microring in the RC network. The results are shown in Fig. 6.

The map of the best BER (top panel) shows an absolute minimum value of about $10^{-1.7}$ and exhibits a region of low values extending for negative detuning frequencies across all the bitrates. Negative detuning is the region where the free carrier nonlinearities are better excited in the microring [16, 21]. Where thermal nonlinearities are excited predominantly and thermal bistability or self-pulsing occur, i.e. positive detuning or high input power, yields BER degradation. The power map (middle panel) exhibits relatively smooth surface, with lower values of power close to the resonance and higher values far from it. Interestingly, the RC network solves the task with low BER when the input bit rate is inversely proportional to the free carrier lifetime (~ 250 Mbps), even though for large input power for positive detunings. The best RB are obtained at several bitrates for negative frequency detunings. On the contrary, for frequency detuning larger than -20 GHz to 30 GHz and input bitrates higher than 800 Mbps, we can observe a region where BER_{out}^b is larger than BER_{in}^b , i.e. the microring resonator nonlinearities do not improve the results of the ridge regression applied on the input optical signal. Analyzing the RB , it looks like that, by exploiting the microring as a memory and nonlinear activation function, there is a clear improve-

ment in performance for negative detunings compared to the case where we just use the inter-symbolic interference and the square module of the response. The latter scenario corresponds to analyzing only the input optical signal.

2. XOR 1 with 2 R-bit and $N_v^d = 5$

Considering the same XOR operation, but with both bits supplied to the ridge regression, we provide the memory needed to solve the operation and the reservoir has only to provide the nonlinearity. The results are shown in Fig. 7.

In this case, the results are much better than in the XOR 1 with 1 R-bit case. The top panel shows a wide region, between 20 and 400 Mbps, in which the BER^b reaches very low values, with an absolute minimum of $10^{-3.4}$. For bitrates of 500 Mbps and above, we can observe a region where the BER^b value does not reach low values (from 10^{-1} to 10^{-2}). The middle panel is similarly divided in two regions, where the one associated with low BER^b values presents higher input power and the one associated with higher BER^b values presents lower input power. It is clear that the system is able to exploit the microring nonlinearities in order to solve the task in the region of high input power, but not in the region of low input power. In this situation, large input powers do not improve the performance calculated on the microring resonator transmitted signal. Again, in the region where the RC network is effective in solving the task, the RB shows a performance increase achieving a ratio of about $10^{2.7}$. Also for this task, we observe that negative detunings are better and allows reaching the statistical limit of the solution as highlighted by the red dots and crosses in the top and bottom panels, respectively. Thus, also in this case, free carrier nonlinearities are used by the RC network.

3. XOR 2-3 with 1-2-3 R-bit and $N_v^d = 5$

Performing the XOR operation on bits separated by two or three bits requires even more memory than the XOR 1 operation and avoid the problem of inter-symbolic interference on the input optical signal. Figure 8 shows results of the XOR 2 operation by showing the map of the ratio between BER_{in}^b and BER_{out}^b when supplying one, two, and three bits to the ridge regression. Whenever $BER_{out}^b < BER_{in}^b$, the task is solved by the nonlinearity of the microring resonator. Note that for the 3 R-bit result, both the bits used in the XOR operation are provided to the ridge regression.

In the first case (top panel), when only the information contained in the current bit is used, the RC network is not able to improve over the bare processing of the input signal. The maximum RB performance increase is $10^{0.2}$. Moreover, apart from the zone contained between 40 and 200 Mbps and with negative frequency detuning,

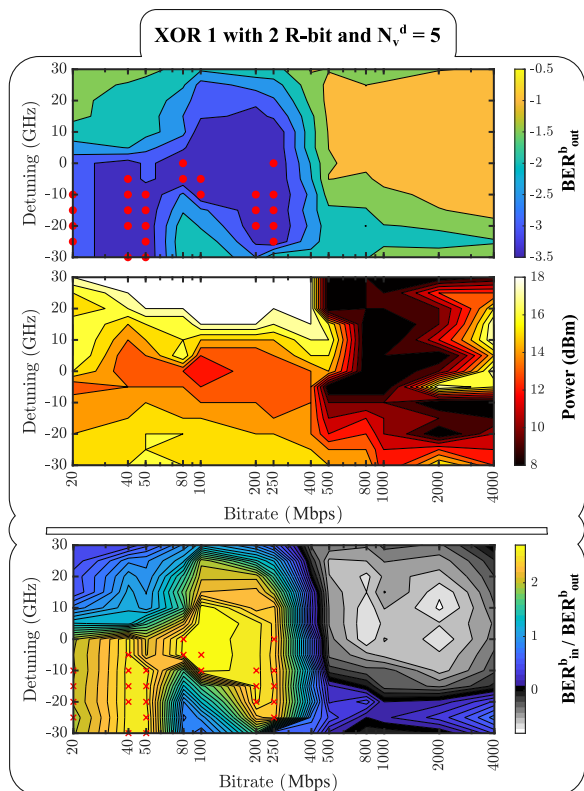


FIG. 7: Same maps of Fig. 3 for XOR 1 with 2 R-bit and $N_v^d = 5$.

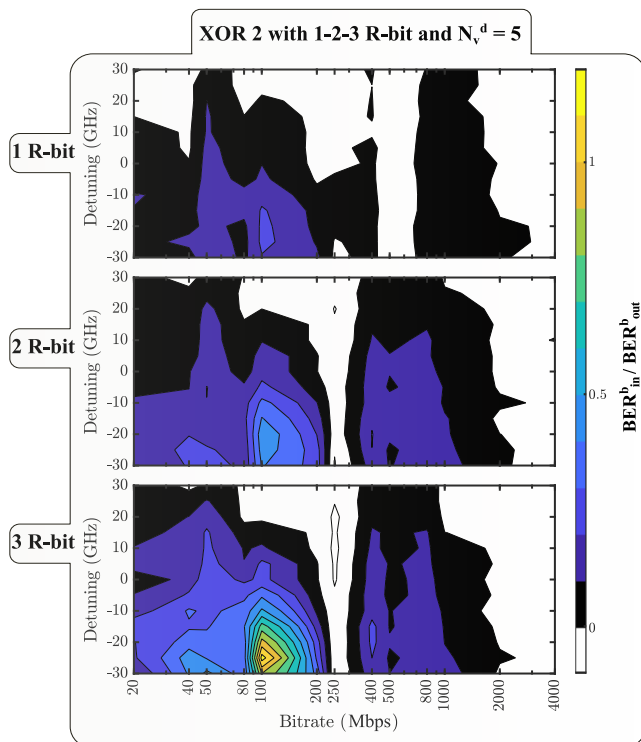


FIG. 8: Map of the ratio between the input and output BER^b as a function of the frequency detuning and bitrate. Specifically, the top, middle and bottom panel shows the experimental results for $N_v^d = 5$ considering the logical operation XOR 2 with 1R-bit, XOR 2 with 2R-bit and XOR 2 with 3R-bit, respectively.

i.e. where the free carrier nonlinearities are effective, the map shows a slight performance decrease.

Interestingly, by providing the ridge regression also with the previous bit ($n_2 = 2$), the region showing performance increase widens and its maximum value becomes about $10^{0.4}$ at a bit rate of 100 Mbps and frequency detuning of -25 GHz. Similarly as before, a second region showing good results appears for negative detuning at 400 and 800 Mbps. By providing all three bits to the ridge regression, the current bit and the previous two, the performance improves conspicuously reaching a maximum ratio RB of $10^{1.1}$ at 100 Mbps, -25 GHz. It looks like

XOR 2	1 R-bit	2 R-bit	3 R-bit
BER_{out}^b	$10^{-0.7}$	$10^{-0.9}$	$10^{-2.6}$
RB	$10^{0.2}$	$10^{0.4}$	$10^{1.1}$

TABLE II: Value of the BER_{out}^b and the corresponding average input optical power at 16 dBm, obtained for a detuning of -25 GHz and a bitrate of 100 Mbps.

that the network efficiently exploits only the nonlinear dynamics of the free carriers in order to solve the logical operation. Table II, allows comparing the RB ratio and BER_{out}^b with each other for 1,2,3 R-bit. In particular, it

reports the BER_{out}^b and the RB ratio for a PRBS signal at a bitrate of 100 Mbps, with an average power equal to 16 dBm, generated by a pump laser at a frequency detuning of -25 GHz.

C. Discussion

The results of “AND 1 with 2 R-bit” provide us the baseline for the discussion: we verify that the ridge regression is able to correctly solve a linear task when provided with the necessary inputs. We do this both using the input optical signal and the reservoir transmitted output optical signals. We observe that the regression reaches the statistical error limit almost everywhere. The task “AND 1 with 1 R-bit” requires to carry the information of the past bit to the current one, exploiting the response of the microring resonator. It appears that this indeed happens in a vast region of the parameter space, mostly for bitrates up to 500 Mbps, and at every frequency detuning, although at different input powers. Similarly, also the “AND 2 with 1 R-bit” task is solved by the RC network, but not at the same performance level as the previous task and for a limited set of parameters. We can therefore summarize the results of the linear tasks by saying that the system is able to provide memory of 1 bit in the past in almost every configurations, memory of 2 bits in past for a restricted set of parameters, and is not able to provide memory of three or more bits in the past. These considerations are validated by the analysis of the maps of RB , which verify that this memory comes indeed by the microring resonator response and not from nonlinearities already imprinted on the input optical signal by the EO conversion. The extension of the memory to just two bits in the past must be seen as the maximum intrinsic performance of the microresonator/bus waveguide system. It does not mean a binding limit. In fact, more memory can be provided a priori by modifying the encoding of virtual nodes [33], or by exploiting a hybridized space-time approach [5]. In this latter, one can vary the reservoir topology, e.g., by coupling spirals to the system, and thus, providing temporal memory between n bits in the past.

The nonlinear tasks, instead, require both memory and nonlinearity. Comparing the results of “XOR 1 with 1 R-bit” and “XOR 1 with 2 R-bit”, we observe that the system struggles to deliver both. In fact, if providing only the current bit to the ridge regression leads to a BER^b of around $10^{-1.7}$ and only for specific combination of the system parameters, with both bits the ridge regression is able to reach the statistical error limit on a wide region. Also in this case, best results are achieved when free carrier nonlinearities are used (i.e. negative detuning and bit rates of 100 Mbps). Moreover, the same can be observed by comparing the maps of RB for “XOR 2” with 1, 2, and 3 R-bits. It is worth noticing that the experimental measurements are based on the nonlinear response encoded within a single signal of a pump laser. As a result,

bits that have a zero value in the PRBS trace do not carry optical energy into the microresonator. Therefore, most of the virtual nodes associated with them are sampled within the background noise. This problem can be solved by exploiting a pump and probe experiment, and then, nonlinearly imprinting the information on a second signal [16]. However, in this work we are not interested in the absolute performance, but rather in the relative trend of the bit rate for the logical operations as a function of the number of bits supplied to the ridge regression in the training procedure.

These results show that both thermal and free carrier nonlinearities impact the performance of the microring reservoir. Specifically, we can see a generalised improvement of RB for bitrates from 100 Mbps to 400 Mbps. These values are close to the inverse of the free carrier lifetime $\sim 1/\tau_{FC} \sim 200$ MHz to 500 MHz. A similar scenario has already been reported by [16], where the higher free carrier lifetime of 45 ns gave rise to best performance around 20 Mbps in the XOR 1 with 1 R-bit task. On the other hand, the interplay of free carrier and thermal nonlinearities, whose lifetime is $\sim 1/\tau_{th} \sim 10$ MHz to 20 MHz, do not deteriorate the device performance if the system is not in a bistable regime. We cannot, however, observe the effect of the thermal nonlinearities alone as it would arise below 20 Mbps. It is good to point out that the photon lifetime, and therefore, the charge and discharge of the microresonator, does not provide memory between the bits. In fact, its effect should occur around a frequency of ~ 200 GHz.

V. CONCLUSION

In this paper, a microresonator coupled to a bus waveguide is exploited as a reservoir in a RC network. The input information is encoded exploiting the temporal approach via virtual nodes, and thus, modulating the amplitude of a single pump laser. The system is trained offline through a ridge regression. By injecting into the bus waveguide a Pseudo Random Binary Sequence dependent on the bitrate, frequency, and average power, we studied linear and nonlinear logic operations, such as AND and XOR. The solution of the first tasks requires memory between the bits on which the logical operation occurs, while that of the second ones requires both: memory and nonlinearity understood as an activation function. Here, we show that a structure as simple as a single microring resonator can already exhibit a complex response, which can be harnessed to yield memory or to nonlinearly transform the signal. In order to distinguish between the two features, we isolated the microring contributions to each

of the two by providing external memory to the ridge regression and by testing linear tasks. The ridge regression succeeds in exploiting the nonlinearity of the microring resonator, either as an activation function, supplying the nonlinear transformation, or for memory, storing information of the past bits into the current one. Furthermore, the single microresonator can induce both memory and nonlinear activation function, overcoming the performance obtained by using the inter-symbolic interference of the input optical signal for tasks which consider the present bit and the past one.

Finally, we observed that, especially in photonic approaches relying on super-sampling and offline analysis, it is critical to know if the input optical signal already contains distortions, created during the modulation, which are enough for the ridge regression to solve the task. Indeed, the optical modulator itself can distort the signal by imprinting spurious nonlinearities and inter-symbolic interference on the optical signal which can then be used by the ridge regression to get the target. Consequently, the virtual node approach requires the analysis of both experimental signals of the reservoir: the input and the output optical signals. Only the knowledge of both allows determining if the system under test provides the necessary nonlinearity to obtain the target. Therefore, it is important to analyze the *RB* values. In other words, solving the task with just the experimental response of the output does not give a concrete proof of the reservoir performance. It only allows stating that the experimental apparatus as a whole system solves the task.

ACKNOWLEDGEMENTS

The authors would like to thank Massimo Borghi for continuous and insightful exchanges and Enrico Moser for technical support.

FUNDING

This project has received funding from the European Research Council (ERC) under the European Union's Horizon 2020 research and innovation programme (grant agreement No 788793, BACKUP), and from the MIUR under the project PRIN PELM (20177 PSCKT).

DISCLOSURES

The authors declare no conflicts of interest.

[1] N. C. Thompson, K. Greenewald, K. Lee, and G. F. Manso, The computational limits of deep learning, arXiv

- [2] X.-W. Chen and X. Lin, Big data deep learning: challenges and perspectives, *IEEE access* **2**, 514 (2014).
- [3] S. Furber, Large-scale neuromorphic computing systems, *Journal of neural engineering* **13**, 051001 (2016).
- [4] R. Nakane, G. Tanaka, and A. Hirose, Reservoir computing with spin waves excited in a garnet film, *Ieee Access* **6**, 4462 (2018).
- [5] S. Sunada and A. Uchida, Photonic neural field on a silicon chip: large-scale, high-speed neuro-inspired computing and sensing, *Optica* **8**, 1388 (2021).
- [6] C. Du, F. Cai, M. A. Zidan, W. Ma, S. H. Lee, and W. D. Lu, Reservoir computing using dynamic memristors for temporal information processing, *Nature communications* **8**, 1 (2017).
- [7] P. A. Merolla, J. V. Arthur, R. Alvarez-Icaza, A. S. Cassidy, J. Sawada, F. Akopyan, B. L. Jackson, N. Imam, C. Guo, Y. Nakamura, *et al.*, A million spiking-neuron integrated circuit with a scalable communication network and interface, *Science* **345**, 668 (2014).
- [8] X. X. Guo, S. Y. Xiang, Y. H. Zhang, L. Lin, A. J. Wen, and Y. Hao, Polarization multiplexing reservoir computing based on a vcsel with polarized optical feedback, *IEEE Journal of Selected Topics in Quantum Electronics* **26**, 1 (2019).
- [9] C. Wu, H. Yu, S. Lee, R. Peng, I. Takeuchi, and M. Li, Programmable phase-change metasurfaces on waveguides for multimode photonic convolutional neural network, *Nature communications* **12**, 1 (2021).
- [10] H. Jaeger, The “echo state” approach to analysing and training recurrent neural networks—with an erratum note, Bonn, Germany: German National Research Center for Information Technology GMD Technical Report **148**, 13 (2001).
- [11] W. Maass and H. Markram, On the computational power of circuits of spiking neurons, *J. Comput. Syst. Sci.* **69**, 593 (2004).
- [12] L. De Marinis, M. Cococcioni, P. Castoldi, and N. Andrioli, Photonic neural networks: A survey, *IEEE Access* **7**, 175827 (2019).
- [13] F. D. Coarer, M. Sciamanna, A. Katumba, M. Freiburger, J. Dambre, P. Bienstman, and D. Rontani, All-optical reservoir computing on a photonic chip using silicon-based ring resonators, *IEEE Journal of Selected Topics in Quantum Electronics* **24**, 1 (2018).
- [14] L. Appeltant, M. C. Soriano, G. Van der Sande, J. Danckaert, S. Massar, J. Dambre, B. Schrauwen, C. R. Mirasso, and I. Fischer, Information processing using a single dynamical node as complex system, *Nature communications* **2**, 1 (2011).
- [15] G. Donati, C. R. Mirasso, M. Mancinelli, L. Pavesi, and A. Argyris, Microring resonators with external optical feedback for time delay reservoir computing (2021), arXiv:2109.11486 [physics.optics].
- [16] M. Borghi, S. Biasi, and L. Pavesi, Reservoir computing based on a silicon microring and time multiplexing for binary and analog operations, *Scientific Reports* **11**, 10.1038/s41598-021-94952-5 (2021).
- [17] M. Borghi, D. Bazzanella, M. Mancinelli, and L. Pavesi, On the modeling of thermal and free carrier nonlinearities in silicon-on-insulator microring resonators, *Optics Express* **29**, 4363 (2021).
- [18] K. Harkhoe, G. Verschaffelt, A. Katumba, P. Bienstman, and G. V. der Sande, Demonstrating delay-based reservoir computing using a compact photonic integrated chip, *Opt. Express* **28**, 3086 (2020).
- [19] J. Bueno, D. Brunner, M. C. Soriano, and I. Fischer, Conditions for reservoir computing performance using semiconductor lasers with delayed optical feedback, *Opt. Express* **25**, 2401 (2017).
- [20] K. Vandoorne, P. Mechet, T. Van Vaerenbergh, M. Fiers, G. Morthier, D. Verstraeten, B. Schrauwen, J. Dambre, and P. Bienstman, Experimental demonstration of reservoir computing on a silicon photonics chip, *Nature Communications* **5**, 3541 (2014).
- [21] T. J. Johnson, M. Borselli, and O. Painter, Self-induced optical modulation of the transmission through a high-q silicon microdisk resonator, *Optics Express* **14**, 817 (2006).
- [22] C. Baker, S. Stapfner, D. Parrain, S. Ducci, G. Leo, E. M. Weig, and I. Favero, Optical instability and self-pulsing in silicon nitride whispering gallery resonators, *Opt. Express* **20**, 29076 (2012).
- [23] Y. Tian, L. Zhang, and L. Yang, XOR/XNOR directed logic circuit based on coupled-resonator-induced transparency, in *Optics and Photonics for Information Processing VII*, Vol. 8855, edited by K. M. Iftikharuddin, A. A. S. Awwal, and A. Márquez, International Society for Optics and Photonics (SPIE, 2013) pp. 187 – 192.
- [24] J.-Y. Kim, J.-M. Kang, T.-Y. Kim, and S.-K. Han, All-optical multiple logic gates with xor, nor, or, and nand functions using parallel soa-mzi structures: theory and experiment, *Journal of Lightwave Technology* **24**, 3392 (2006).
- [25] Y. Tian, D. Li, Z. Liu, H. Xiao, G. Zhao, J. Yang, Y. Zhao, G. Han, and X. Gao, Simulation and demonstration of directed xor/xnor logic gates using two cascaded microring resonators, *IEEE Photonics Journal* **8**, 1 (2016).
- [26] S. Biasi, P. Guillemé, A. Volpini, G. Fontana, and L. Pavesi, Time response of a microring resonator to a rectangular pulse in different coupling regimes, *Journal of Lightwave Technology* **37**, 5091 (2019).
- [27] W. H. P. Pernice, C. Schuck, M. Li, and H. X. Tang, Carrier and thermal dynamics of silicon photonic resonators at cryogenic temperatures, *Opt. Express* **19**, 3290 (2011).
- [28] Q. Xu and M. Lipson, All-optical logic based on silicon micro-ring resonators, *Optics express* **15**, 924 (2007).
- [29] V. R. Almeida, C. A. Barrios, R. R. Panepucci, and M. Lipson, All-optical control of light on a silicon chip, *Nature* **431**, 1081 (2004).
- [30] L.-W. Luo, G. S. Wiederhecker, K. Preston, and M. Lipson, Power insensitive silicon microring resonators, *Optics letters* **37**, 590 (2012).
- [31] T. Van Vaerenbergh, M. Fiers, J. Dambre, and P. Bienstman, Simplified description of self-pulsation and excitability by thermal and free-carrier effects in semiconductor microcavities, *Phys. Rev. A* **86**, 063808 (2012).
- [32] T. V. Vaerenbergh, M. Fiers, P. Mechet, T. Spuesens, R. Kumar, G. Morthier, B. Schrauwen, J. Dambre, and P. Bienstman, Cascadable excitability in microrings, *Opt. Express* **20**, 20292 (2012).
- [33] S. Ortín, M. C. Soriano, L. Pesquera, D. Brunner, D. San-Martín, I. Fischer, C. R. Mirasso, and J. M. Gutiérrez, A unified framework for reservoir computing and extreme learning machines based on a single time-delayed neuron, *Scientific Rep.* **5**, 14945 (2015).